INTERFEROMETRIC PARTICLE SIZING

D. W. Roberds, B. W. Bomar, and R. W. Menzel
ARO, Inc., a Sverdrup Corporation Company

ARNOLD ENGINEERING DEVELOPMENT CENTER
AIR FORCE SYSTEM COMMAND
ARNOLD AIR FORCE STATION, TENNESSEE 37389

April 1978

Final Report for Period September 1976 - April 1977

Prepared for

ARNOLD ENGINEERING DEVELOPMENT CENTER/DOTR
ARNOLD AIR FORCE STATION, TENNESSEE 37389

NOTICES
When U. S. Government drawings, specifications, or other data are used for any purpose other than a definitely related Government procurement operation, the Government thereby incurs no responsibility nor any obligation whatsoever, and the fact that the Government may have formulated, furnished, or in any way supplied the said drawings, specifications, or other data, is not to be regarded by implication or otherwise, or in any manner licensing the holder or any other person or corporation, or conveying any rights or permission to manufacture, use, or sell any patented invention that may in any way be related thereto.
Qualified users may obtain copies of this report from the Defense Documentation Center.
References to named commerical products in this report are not to be considered in any sense as an indorsement of the product by the United States Air Force or the Government.

This report has been reviewed by the Information Office (OI) and is releasable to the National Technical Information Service (NTIS). At NTIS, it will be available to the general public, including foreign nations.

APPROVAL STATEMENT

This report has been reviewed and approved.

Marshall K. Kingery

MARSHALL K. KINGERY
Project Manager, Research Division
Directorate of Test Engineering

Approved for publication:

FOR THE COMMANDER

Marion L. Laster

MARION L. LASTER
Director of Test Engineering
Deputy for Operations

REPORT DOCUMENTATION PAGE		READ INSTRUCTIONS BEFORE COMPLETING FORM
1 REPORT NUMBER AEDC-TR-77-116	2 GOVT ACCESSION NO.	3. RECIPIENT'S CATALOG NUMBER
4 TITLE (and Subtitle) INTERFEROMETRIC PARTICLE SIZING		5 TYPE OF REPORT & PERIOD COVERED Final Report-September 1976 - April 1977 6 PERFORMING ORG. REPORT NUMBER
7 AUTHOR(s) D. W. Roberds, B. W. Bomar, and R. W. Menzel, ARO, Inc.		8 CONTRACT OR GRANT NUMBER(s)
9 PERFORMING ORGANIZATION NAME AND ADDRESS Arnold Engineering Development Center/DOT Air Force Systems Command Arnold Air Force Station, Tennessee 37389		10. PROGRAM ELEMENT, PROJECT, TASK AREA & WORK UNIT NUMBERS Program Element 65807F
11. CONTROLLING OFFICE NAME AND ADDRESS Arnold Engineering Development Center/DOS Arnold Air Force Station, Tennessee 37389		12. REPORT DATE April 1978 13. NUMBER OF PAGES 38
14 MONITORING AGENCY NAME & ADDRESS(if different from Controlling Office)		15 SECURITY CLASS. (of this report) UNCLASSIFIED 15a DECLASSIFICATION/DOWNGRADING SCHEDULE N/A

16. DISTRIBUTION STATEMENT (of this Report)

Approved for public release; distribution unlimited.

17 DISTRIBUTION STATEMENT (of the abstract entered in Block 20, if different from Report)

18. SUPPLEMENTARY NOTES

Available in DDC

19. KEY WORDS (Continue on reverse side if necessary and identify by block number)

interferometry
laser velocimeters
particle size
spheres
beam splitting
polarization
scattering

20 ABSTRACT (Continue on reverse side if necessary and identify by block number)

The theory and experimental conditions are summarized under which single, spherical particles in the size range of a few micrometers and larger may be accurately sized using the observed fringe visibility in a crossed-beam laser velocimeter. Scalar diffraction theory and experimental data are presented to show how the size information in the forward scattered light is dependent on the collection optics geometry, including the size

DD FORM 1 JAN 73 1473 EDITION OF 1 NOV 65 IS OBSOLETE

20. ABSTRACT (Continued)

and shape of source beam stops. The scattered light signal waveform is analyzed in both the time and frequency domains, and electronic instrumentation is outlined for rapid acquisition of size data.

AFSC
Arnold AFS Tenn

PREFACE

The work reported herein was conducted by the Arnold Engineering Development Center (AEDC), Air Force Systems Command (AFSC), under Program Element 65807F. The results were obtained by ARO, Inc., AEDC Division (a Sverdrup Corporation Company), operating contractor for the AEDC, AFSC, Arnold Air Force Station, Tennessee, under ARO Project No. B32I-02A. Marshall K. Kingery was the Air Force project monitor. The manuscript was submitted for publication on November 2, 1977.

CONTENTS

ILLUSTRATIONS

Figure

Figure | Page

APPENDIXES

1.0 INTRODUCTION

It has been shown that particle size information is inherent in the scattered light when a single particle passes through the probe volume of a laser interferometer of the type used in crossed-beam laser velocimetry (Ref. 1). It has also been shown, through scalar diffraction analysis, that this size information is dependent on the collection optics geometry (Ref. 2 and 3). An analysis of the scattered light signal using Mie theory for scattering from spheres also shows the dependence on the collection optics geometry as well as other parameters (Ref. 4 and 5). A recent paper (Ref. 6) reports determination of size distributions in the range of 2 to 10 micrometers, using Mie theory and a small light collection aperture located off-axis in the forward direction.

The goal of the research reported here was twofold: first, to establish by a theoretical and experimental study the relationship between the scattered light waveform and the scattering particle diameter, including such parameters as the size of the light collection aperture and source beam stops: and second, to design a practical, accurate particle-sizing system for Arnold Engineering Development Center (AEDC) applications. The results of the theoretical and experimental study are presented in Section 2.0 which includes (1) a brief review of the theory of single-particle interferometric sizing, (2) results based on theory and experimental data which show the effects of the collection optics geometry on the forward-scattered light waveform, and (3) experimental data to show that the visibility method of sizing does not appear to be applicable in a backscatter mode, at least in the range of sizes examined, which were much larger than the illuminating wavelength.

The subject of Section 3.0 is a time and frequency domain analysis of particle-sizing interferometer signals. Such an analysis is a prerequisite for design of signal processing electronics.

The subject of Section 4.0 is the design of an electronic processor for recording the visibility of the signals for subsequent particle size analysis.

The findings of this report are summarized in Section 5.0.

2.0 INTERFEROMETRIC PARTICLE SIZE ANALYSIS: RELATION OF VISIBILITY TO PARTICLE SIZE

2.1 THEORY OF SINGLE-PARTICLE INTERFEROMETRIC SIZING

An optical arrangement for generating a set of high-contrast fringes is shown in Fig. 1. The laser beam (assumed to be in the TEM_{00} mode) is split into two beams which are then caused by lenses to both cross and focus at a common point. The two beams are of

equal intensity and linearly polarized in the same direction. At the crossing point, each beam focuses to a waist characterized by planar wavefronts. A coordinate system is defined (shown in Fig. 1) such that z lies along the bisector of the beams, x is in their direction of polarization, y is in the plane of the beams, and the origin is at the crossing point of the beams.

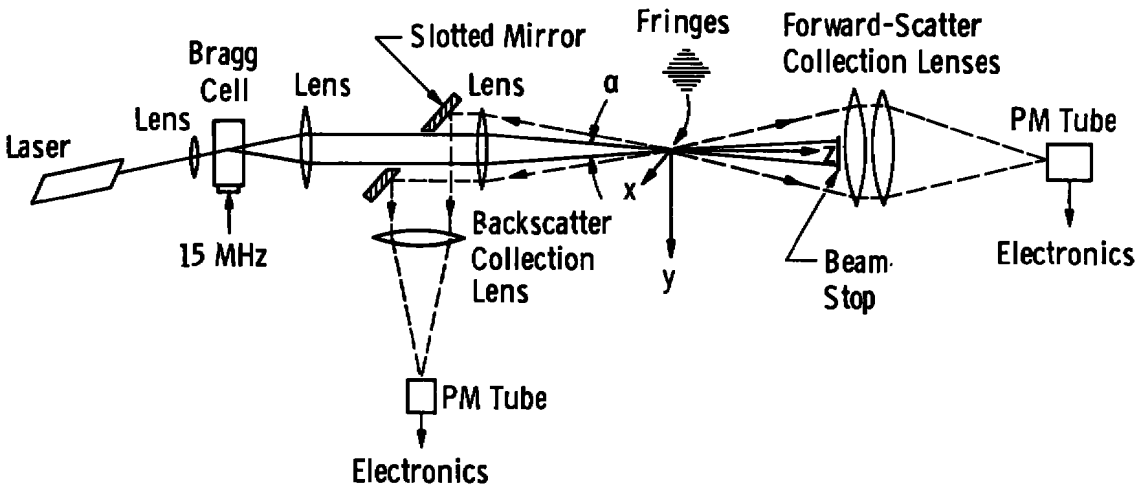

Figure 1. Schematic of optical system.

The splitting of the beams is accomplished either by beam-splitting glass blocks, which produce stationary fringes in the region where the beams cross, or by a Bragg cell, which produces moving fringes. In the Bragg cell, ultrasonic sound waves in water diffract the incoming beam such that the output contains a zero-order (undiffracted) beam and a higher order beam which is changed in its propagation direction and changed in its frequency by an amount equal to the frequency of the sound waves.

Assuming for simplicity that glass blocks, rather than a Bragg cell, are used, let the electric fields E_1 and E_2 of the two laser beams in the region of crossover be expressed (Ref. 7) as

$$E_1 = E_o \exp\left[-(x_1^2 + y_1^2)/b_o^2\right] \exp\left[-i\omega_o t + ikz_1\right] \quad (1a)$$

$$E_2 = E_o \exp\left[-(x_2^2 + y_2^2)/b_o^2\right] \exp\left[-i\omega_o t + ikz_2\right] \quad (1b)$$

where E_o is the field magnitude on the centerline of each beam, b_o is the beam waist radius, ω_o is the optical radian frequency, and $k = 2\pi/\lambda_o$, where λ_o is the optical wavelength. Each electric field is expressed in terms of its own coordinate system referred to its own direction of propagation: z_i is in the direction of propagation of the "i^{th}" beam, x_i is in the direction of polarization, and y_i is orthogonal to the $x_i z_i$ plane. The origin of each of these coordinate systems is also located at the crossing point of the two beams. Since the beams are polarized in the same direction, all the x-axes coincide, i.e., $x_1 = x_2 = x$.

The two plane wave radiations interfere to form interference fringe planes which lie parallel to the xz plane with spacing δ equal to

$$\delta = \lambda_o/(2 \sin(\alpha/2)) \tag{2}$$

where α is the angle formed by the crossed beams.

Collection lenses collect the light scattered from a particle which passes through the fringe system (the "probe volume"), and a photodetector is used to detect the optical signal. Figure 1 outlines optics for collecting the light scattered in the on-axis forward direction, where scalar diffraction analysis may be conveniently applied, and in the on-axis backward direction, where analysis is more complicated, being based, for example, on Mie scattering theory. It should be noted that when forward-scattered light is collected the laser source beams must be avoided, as by the use of a beam stop or stops, as shown in Fig. 1.

Before considering the mathematical analysis of the scattered light signal, it is appropriate to give a heuristic description of how the optical signal may be expected to be dependent on the particle size. If the particle crossing the fringes is very small compared to the fringe spacing, the scattered light signal is closely proportional to the incident intensity at the location of the particle. The detected optical signal will simply reproduce the incident intensity distribution, as shown in Fig. 2a, which shows a reproduction of the photodetector output current versus time for a small particle passing through the crossing point of the beams. If, however, the particle is comparable in size to the spacing between the fringes, the particle will always partially overlap bright fringes even when it is centered in a dark fringe, and it should be expected that the scattered power will never fall to zero while the particle is crossing the fringes. This is shown in Fig. 2b. A still larger particle will overlap yet more of the adjacent fringes during its traversal and might produce the signal shown in Fig. 2c. Thus the relative amount of oscillation in the scattered light signal, i.e., the "visibility" of the fringes in the detected signal, may be expected to be a function of the size of the particle relative to the fringe spacing. As shown in Fig. 2b, the signals are comprised of an oscillating component,

called the "a-c", and a lower frequency component called the "pedestal." The visibility at a point on the waveform is defined as the ratio of the a-c magnitude to the pedestal at that point.

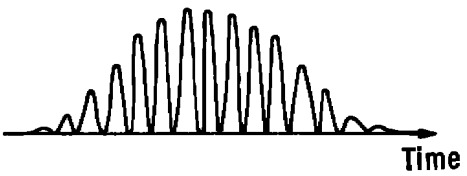

a. Visibility = 1.0

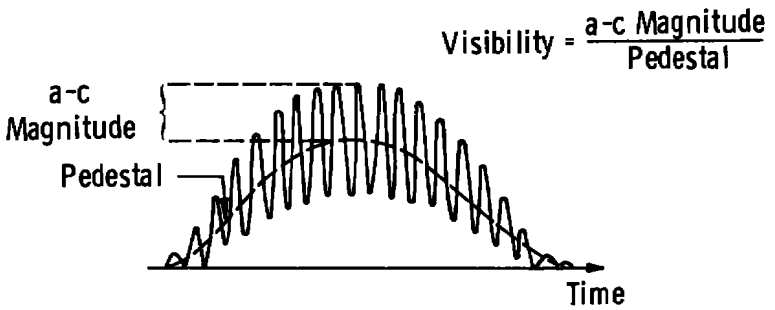

b. Visibility = 0.47

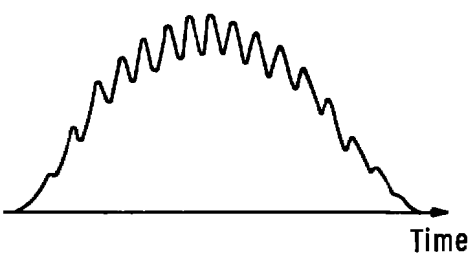

c. Visibility = 0.12

Figure 2. Photodetector output signal for three values of D/δ, z = 0.

A scalar analysis of the forward-scattered light signal is formulated by calculating the fields, E_{s1} and E_{s2}, diffracted by a particle from each of the illuminating beams. The two diffracted fields are then summed in the plane of the collection lens to find the total field E_s:

$$E_s = E_{s1} + E_{s2} \tag{3}$$

The intensity I of the total diffracted field is calculated as

$$I = \frac{1}{2\eta} E_s E_s^*$$

$$= \frac{1}{2\eta} \left\{ \left| E_{s1} \right|^2 + \left| E_{s2} \right|^2 - 2 \left| E_{s1} \right| \left| E_{s2} \right| \cos \gamma \right\} \tag{4}$$

where * denotes the complex conjugate, $|E_{s1}|$ and $|E_{s2}|$ denote the magnitudes of the complex quantities E_{s1} and E_{s2}, γ is the phase difference between E_{s1} and E_{s2}, and η is the wave impedance of the surrounding medium.

The total power collected by the collection lens and transmitted to the photodetector is found by integrating the intensity over the effective aperture of the collection lens. The photodetector output current i_p is proportional to this collected power:

$$i_p \sim \iint_{\substack{\text{col} \\ \text{lens}}} \left\{ \left| E_{s1} \right|^2 - \left| E_{s2} \right|^2 + 2 \left| E_{s1} \right| \left| E_{s2} \right| \cos \gamma \right\} da \tag{5}$$

where da is an element of area on the collection lens.

Analogous equations to those above may be used in the vectorial formulation of the problem using Mie theory, where the integral over the collection lens is represented by an integration over a solid angle of collection, rather than over a plane area.

In the photodetector output current given above, the terms

$$\iint \left\{ \left| E_{s1} \right|^2 + \left| E_{s2} \right|^2 \right\} da \tag{6}$$

represent the pedestal component, whereas the oscillating a-c component is given by

$$2 \cos \gamma \iint \left| E_{s1} \right| \left| E_{s2} \right| da \tag{7}$$

(Analysis shows that the quantity γ does not depend on the coordinates of integration and therefore may be removed from the integral.) The ratio of the magnitude of the a-c oscillation to the pedestal is defined as the visibility V:

$$V = \frac{2 \iint \left| E_{s1} \right| \left| E_{s2} \right| da}{\iint \left\{ \left| E_{s1} \right|^2 + \left| E_{s2} \right|^2 \right\} da} \tag{8}$$

This definition of the visibility differs slightly from the usual definition of the Michelson visibility function (Ref. 8). Michelson's definition is based on the maximum intensity in a bright fringe and the minimum intensity in an adjacent dark fringe, whereas the above definition ratios the magnitude of the a-c envelope to the pedestal at one location on the waveform. If a stationary particle and moving fringes are assumed so that the intensity maximum in a bright fringe and the minimum in a dark fringe can be measured at the same particle location, then the two definitions are equivalent.

An analysis based on Fraunhofer diffraction is given in Appendix A. The Gaussian shape of the intensity distribution in each illuminating beam is taken into consideration to the extent necessary to show how the observed optical signal varies with the particle's position in the probe volume. The diffraction geometry is shown in Figure 3.

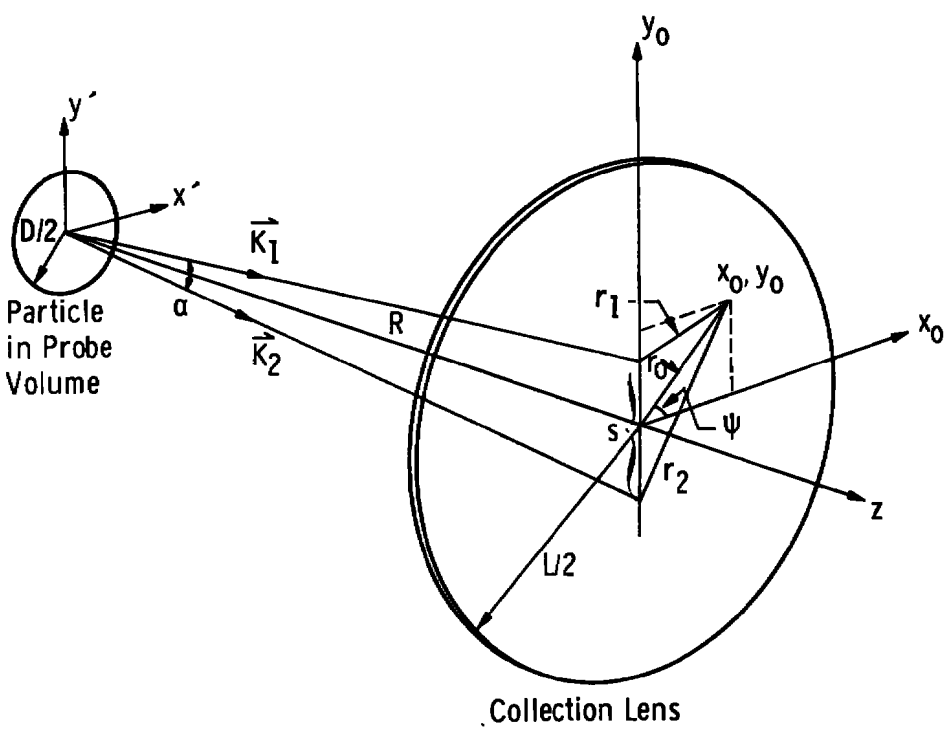

Figure 3. Diffraction geometry.

Assumptions made in the analysis are as follows:

1. The fields illuminating the scattering particle are given by the fields of Eq. (1).

2. The scattering particle is a sphere whose diameter D is much smaller than the beam waist diameter $2b_o$, so that the Gaussian intensity variation in each illuminating beam may be taken as constant across the face of the particle.

3. The distance R from the beam crossing point to the light collection lens is large compared with the extent of the probe volume, so that the diffracted fields at the collection lens may be calculated as though they originate at the geometric crossing point. The displacement of the scattering particle from probe center will be taken into consideration only to account for the varying incident intensity distribution in the probe volume.

In addition, the usual assumptions are made in order to apply Fraunhofer diffraction (Ref. 9); i.e., the sphere diameter D is assumed large compared with the illuminating wavelength λ_o and the diffracted light is observed near the optical axis of each beam (requiring that the beam separation angle a be small) in a region where $R >> D^2/\lambda_o$. The requirement that a be small permits substituting a for sin a and unity for cos a in the analysis.

The results of the analysis show that for a circular collection lens centered on the optical axis, the photodetector output current is given by

$$i_p \sim \exp\left[-\frac{2}{b_o^2}\left(x^2 - y^2 + z^2 a^2/4\right)\right] \left[\cosh\left(2\,yz\,a/b_o^2\right) + V_o \cos\left(2\pi y/\delta\right)\right] \tag{9}$$

where

$$V_o = \frac{2\int_0^{2\pi}\int_0^{L/2} \frac{J_1(\beta r_1)}{(\beta r_1)} \frac{J_1(\beta r_2)}{(\beta r_2)}\, r_o\, dr_o\, d\psi}{\int_0^{2\pi}\int_0^{L/2} \left[\frac{J_1^2(\beta r_1)}{(\beta r_1)^2} + \frac{J_1^2(\beta r_2)}{(\beta r_2)^2}\right] r_o\, dr_o\, d\psi} \tag{10}$$

and where x, y, z are the coordinates of the particle's location in the probe volume, J_1 is a first-order Bessel function of the first kind, $\beta = \pi(D/\delta)/s$, s is the distance between the points where the source beams strike the collection lens ($\simeq$ R a), r_1, r_2 are identified in Fig. 3 as radial distances on the lens from these points. L is the collection lens diameter, and r_o, ψ are circular coordinates centered on the collection lens.

To perform the integration, r_1 and r_2 are written in terms of r_o and ψ

$$r_1^2 = r_o^2 + (s^2/4) - r_o\, s \sin \psi$$

$$r_2^2 = r_o^2 + (s^2/4) + r_o\, s \sin \psi$$

In Eq. (10), the limits of integration are shown to include the entire collection lens. When the effect of beam stops is to be taken into account, the limits of integration must be chosen to exclude the area blocked by the stops.

The visibility may be written using Eq. (8) and results given in Appendix A, or may be written simply from Eq. (9) as the ratio of the cosine magnitude to the pedestal:

$$V = \frac{V_o}{\cosh (2\, yz\alpha/b_o^2)} \tag{11}$$

This result shows that the visibility may vary from point to point along the signal waveform, depending on the particle's y and z coordinates in the probe volume. This information is particularly important for systems designed to size moving particles. From Eq. (11) it may be seen that in either the z = 0 plane or the y = 0 plane (which represent regions of maximum interference between the illuminating beams) the cosh term is reduced to unity, and the visibility reaches a maximum given by V_o. Therefore, if the particle is known to pass through one of these planes, the maximum visibility V_o may be measured and related to the particle size. It is shown in Ref. 2 that when all of the forward diffracted light from a spherical particle is collected, (as with a lens of infinite diameter with no beam stops) the visibility V_o can be expressed in closed form as

$$V_o = \frac{2J_1 (\pi D/\delta)}{(\pi D/\delta)} \tag{12}$$

an expression previously obtained in Ref. 1. Although diffraction analysis leads to different results when not all the diffracted light is collected, Eq. (12) is nevertheless useful for comparison purposes.

2.2 VARIATIONS IN THE VISIBILITY VERSUS D/δ CURVE FOR PRACTICAL COLLECTION APERTURES

The expression for V_o given by Eq. (10) may be written for convenience in a slightly different form, by making the change of variable $u = r_o/s$:

$$V_o = \frac{2 \int_0^{2\pi} \int_0^{(L/2)/s} \frac{J_1 (\beta r_1)}{(\beta r_1)} \frac{J_1 (\beta r_2)}{(\beta r_2)}\, u\, du\, d\psi}{\int_0^{2\pi} \int_0^{(L/2)/s} \left[\frac{J_1^2 (\beta r_1)}{(\beta r_1)^2} + \frac{J_1^2 (\beta r_2)}{(\beta r_2)^2} \right] u\, du\, d\psi} \tag{13}$$

where βr_1 and βr_2 are given by

$$\beta r_1 = (\pi D/\delta)\ (u^2 + \tfrac{1}{4} - u \sin \psi)^{\frac{1}{2}}$$

$$\beta r_2 = (\pi D/\delta)\ (u^2 + \tfrac{1}{4} + u \sin \psi)^{\frac{1}{2}}$$

The visibility V_o now depends only on the ratio D/δ of particle diameter to fringe spacing, and on the limits of integration defining the light collection aperture. The radial limit of integration is a dimensionless lens radius given by the ratio of the actual radius L/2 to the distance s between the source beams at the lens.

The variation of the visibility with size of the collection aperture, when the beam stops are neglected, has been reported previously (Ref. 2). This variation is presented in a different form in Fig. 4, which contains plots of the visibility V_o versus D/δ. The first

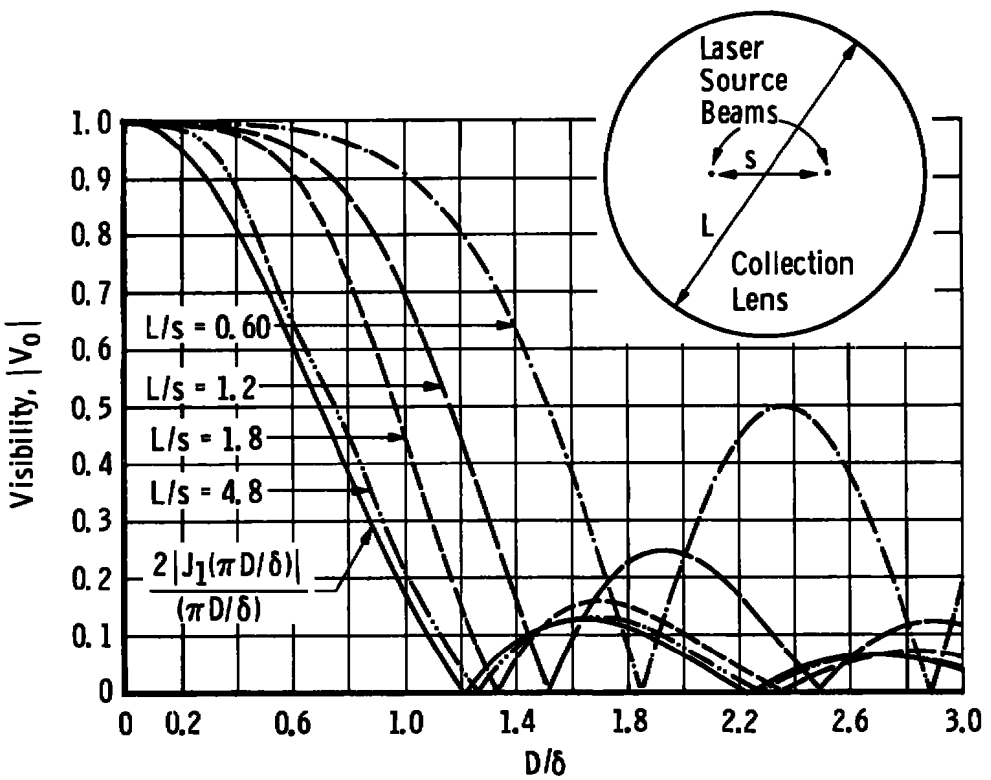

Figure 4. Visibility versus D/ δ for different values of L/s, the ratio of the collection lens diameter to beam separation at the lens, neglecting beam stops.

curve shown (the solid line) is a plot of Eq. (12), the theoretical case where all of the diffracted light is collected. Each of the other curves represents a different collection aperture size, given in terms of the ratio L/s of the lens diameter to the distance between the source beams at the lens. The curve for L/s = 0.60 represents a case where the diffracted light is collected only in a small circular region between the beams. It can be seen that as the ratio L/s is made smaller, the slope of the curve flattens at the lower size range and the region increases where there is an ambiguity caused by different particle sizes having the same visibility. The consequence is that when the fringe spacing is decreased (larger a) to measure smaller particles, s is increased and a proportionately large collection aperture L is required.

In a practical system, the effect of the beam stop or stops cannot be neglected as in the previous analyses. The curves of Fig. 5 show variation in the visibility versus D/δ curves with the size of a single, circular beam stop located at the center of the collection lens. This beam stop configuration is presented in Fig. 5, where the stop is large enough

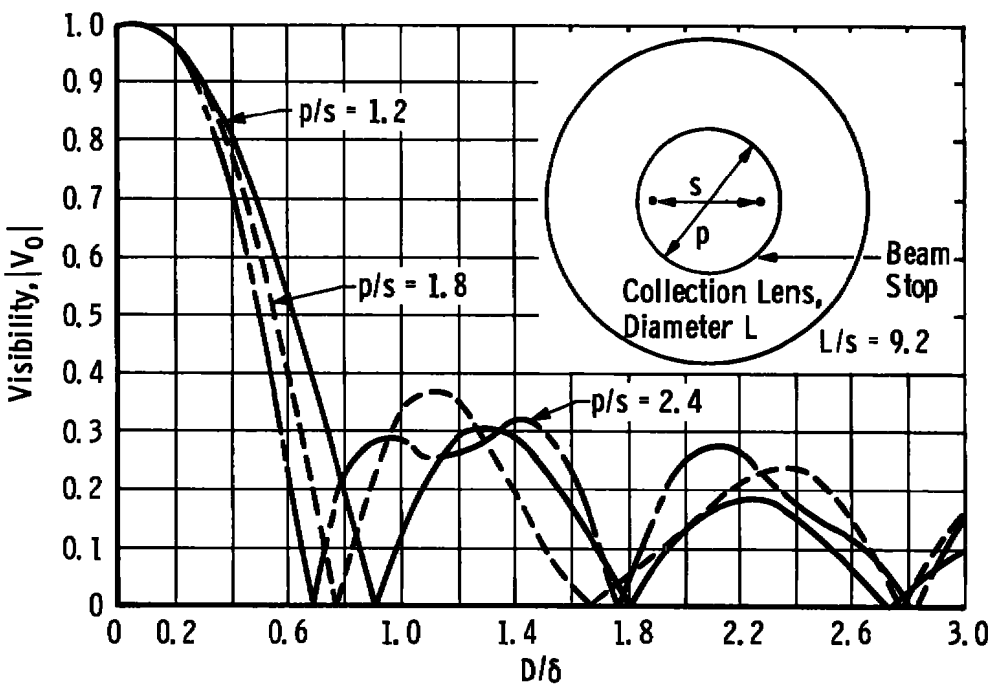

Figure 5. Visibility versus D /δ for various values of p/s, the ratio of the beam stop diameter to beam separation at the lens for a single, circular beam stop at center of collection lens.

to block both source beams. For this case, Eq. (13) was evaluated with the lower radial limit of integration changed from zero to (p/2)/s, where p/2 is the radius of the beam stop. Each curve represents a different value of beam stop size, given in terms of the ratio p/s of the stop diameter to the distance between the beams. For the computation of each curve, the upper radial limit of integration corresponded to a large receiving aperture with L/s = 9.2.

None of the curves of Fig. 5 is very useful for sizing, since there is an ambiguity in determining size for values of the visibility less than about 0.3. More suitable curves can be obtained by using two smaller, circular beam stops, each of diameter p, one centered on each source beam, as presented in Fig. 6. The curves shown in Fig. 6 were obtained by appropriately changing the limits of integration in Eq. (13) for such twin beam stops. Each curve represents a different value of beam stop size, given in terms of the ratio of the individual stop diameter p to the distance s between stop centers. It can be seen that in these curves the ambiguity in determining the size occurs at much lower values of the visibility than in the curves of Fig. 5.

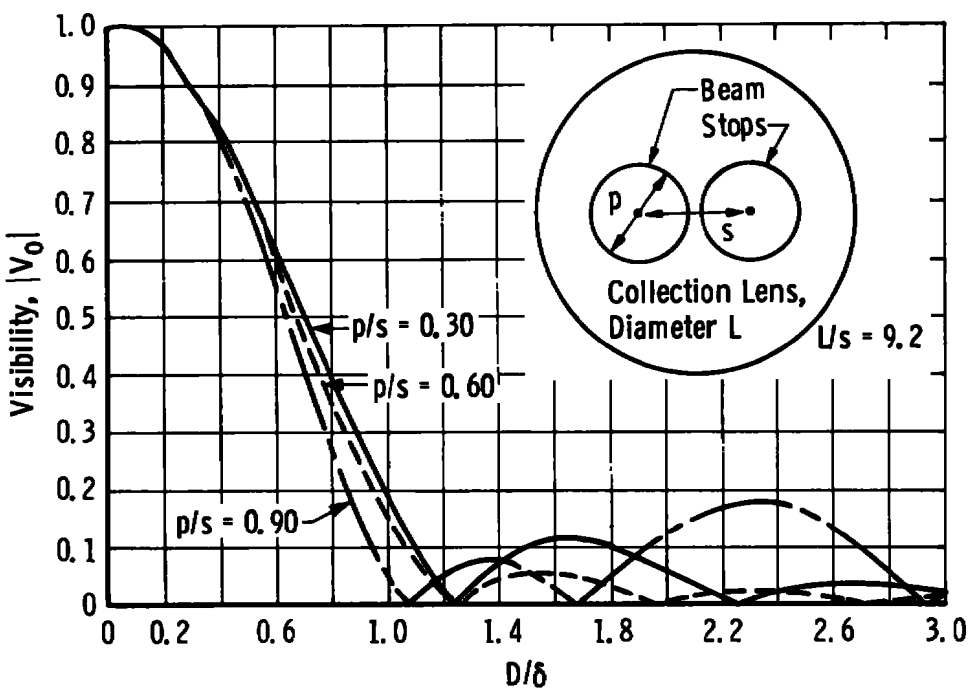

Figure 6. Visibility versus D/ δ for various values of p/s, the ratio of beam stop diameter to the beam separation at the lens for a twin beam stop configuration.

2.3 EXPERIMENTAL DATA - FORWARD SCATTER

Experimental data were taken for comparison with the computed curves for different beam stop configurations. The optical arrangement used is schematically shown in Fig. 1, using the forward-scatter collection optics. The light source was a low-power, helium-neon laser. A Bragg cell beam splitter driven at 15 MHz produced moving fringes in the crossover region of the two beams. A 6-in.-diam, F/5 collection lens was located on-axis, and the optical signal was detected by an RCA Type 8644 photomultiplier (PM) tube. The PM tube output was monitored by a Tektronix Model 7623A storage oscilloscope and by an electronic processor specially designed (Ref. 3) to measure the visibility of the waveforms. The fringe spacing was calculated from a measure of the angle between the beams. Visibility measurements were made for spherical glass beads and for water droplets. Some additional data were also taken for commercially obtained circular apertures of specified diameters cut into an opaque screen for comparison with the theory.

The glass beads were placed on a glass slide and then inserted into the probe volume. There was no requirement to move the particle except to center it in the probe volume, since the fringes were moving to generate the optical signal. The glass spheres were individually observed on the slide using an optical microscope. For comparison with the visibility measurements, some glass spheres were sized by using a microscope with a calibrated reticle, while others were sized by measuring the distance from the center to the first zero in the single beam diffraction pattern.

The water droplets were generated by a Berglund-Liu aerosol generator, which produces a stream of monodisperse droplets (Ref. 10). The stream was observed using an optical microscope and a strobe light, and the droplets were observed to be highly uniform. The diameter of the droplets could be varied and their size was calculated for comparison with the visibility measurements by using the generator's liquid flow rate and the frequency with which the droplets were formed.

The data for the glass spheres are plotted in Fig. 7, along with the theoretically predicted curves. The closed symbols are for a single, central beam stop, and the open symbols are for a twin beam stop configuration. The squares represent the spherical glass beads, and the circles represent data obtained using the circular apertures. Very good agreement with theory was obtained for both the central beam stop and for the twin beam stop cases. Data for the water droplets are shown in Fig. 8 where twin beam stop configuration was used.

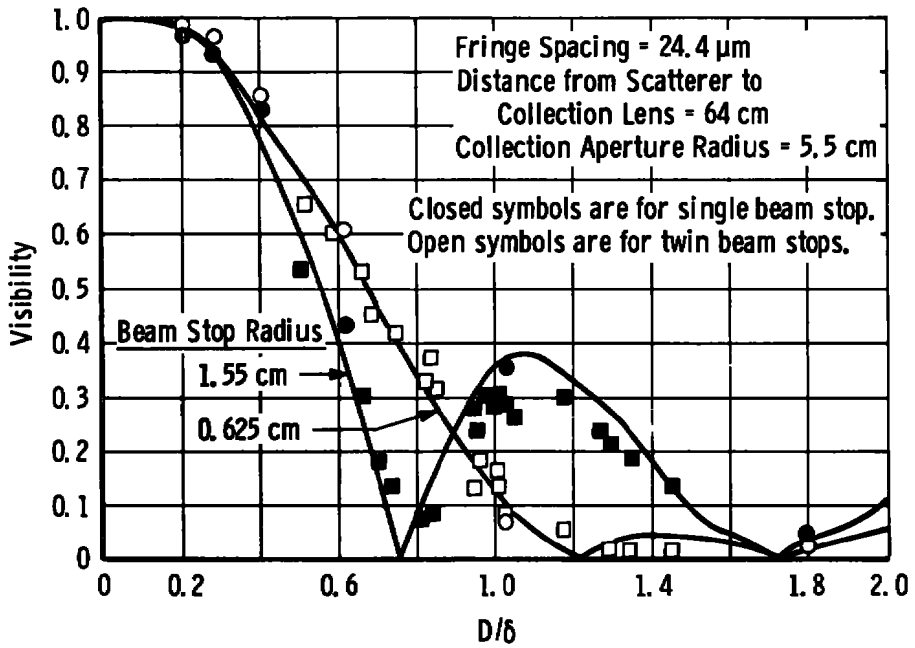

Figure 7. Theoretical and experimental comparison for a single beam stop and for twin beam stops.

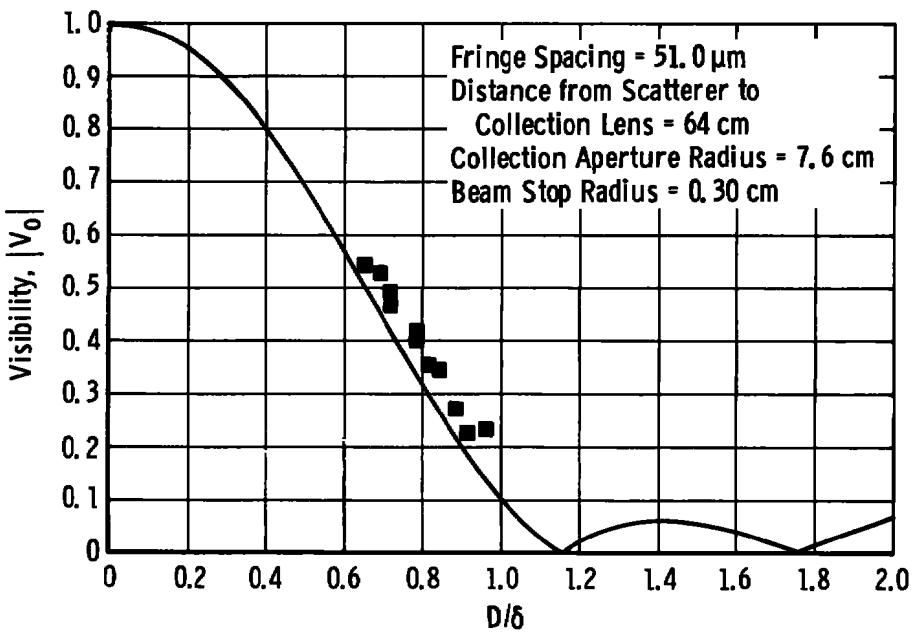

Figure 8. Theoretical and experimental comparison for a twin beam stop configuration using water drops.

2.4 EXPERIMENTAL DATA - BACKSCATTER

Visibility data were also taken for the glass spheres and the water droplets, using the backscatter collection optics shown in Fig. 1. The purpose was to obtain an experimental curve relating the visibility to D/δ for spheres. A theoretical prediction for the backscattered visibility versus D/δ curve for a specific receiving geometry has not yet been worked out, although Adrian and Earley (Ref. 4) have performed a related analysis of the scattered light signal of a crossbeam laser velocimeter using Mie theory. They showed that the backscattered light signal is dependent on particle index of refraction and polarization effects as well as on the receiving aperture geometry, the particle diameter, and the fringe spacing.

Backscatter data for glass spheres ranging in diameter from 19 to 103 μm are shown in Fig. 9. The curve shown is the curve of Eq. (12), included only as a reference, and should not be interpreted as a theoretical prediction. Comparing the data in Fig. 9 with Fig. 7, the most significant thing to note is the wide variation in Fig. 9 in measured visibilities for spheres of approximately the same size. Whereas the measured visibilities in the forward-scattered system were well-behaved and fell close to the theoretically predicted curve, the backscattered visibilities were much less well-behaved.

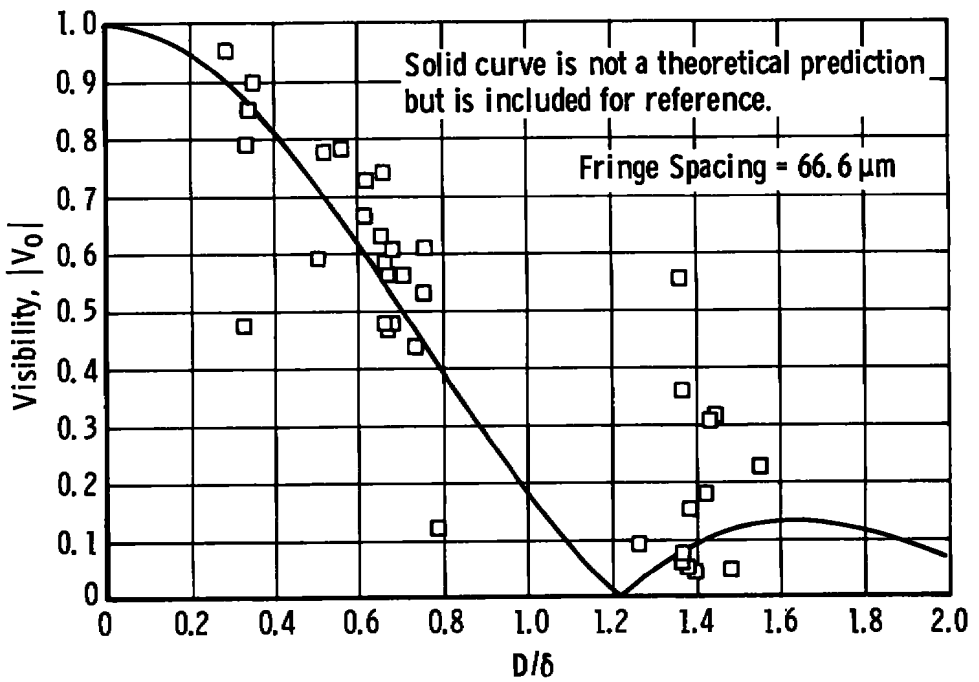

Figure 9. Backscatter data for spherical glass beads.

Backscatter data were also obtained for water droplets ranging in diameter from 34 to 46 μm produced by the Berglund-Liu generator. Two fringe spacings were used to produce values of D/δ from 0.51 to 1.21. Here the variation in the measured visibility for each value of D/δ was most graphic. The visibilities in the forward-scatter direction from the droplets were uniformly well-behaved and remained close to the theoretical prediction as in Fig. 8. Observation of the stream with a microscope and strobe light further showed uniformly spherical droplets of the same size. However, the observed backscattered visibilities of successive, monodisperse droplets underwent a slow, cyclic, relatively wide variation. The extent of this variation for each value of D/δ is shown in Fig. 10 by the vertical lines. The curve shown in Fig. 10 is again simply the reference curve of Eq. (12).

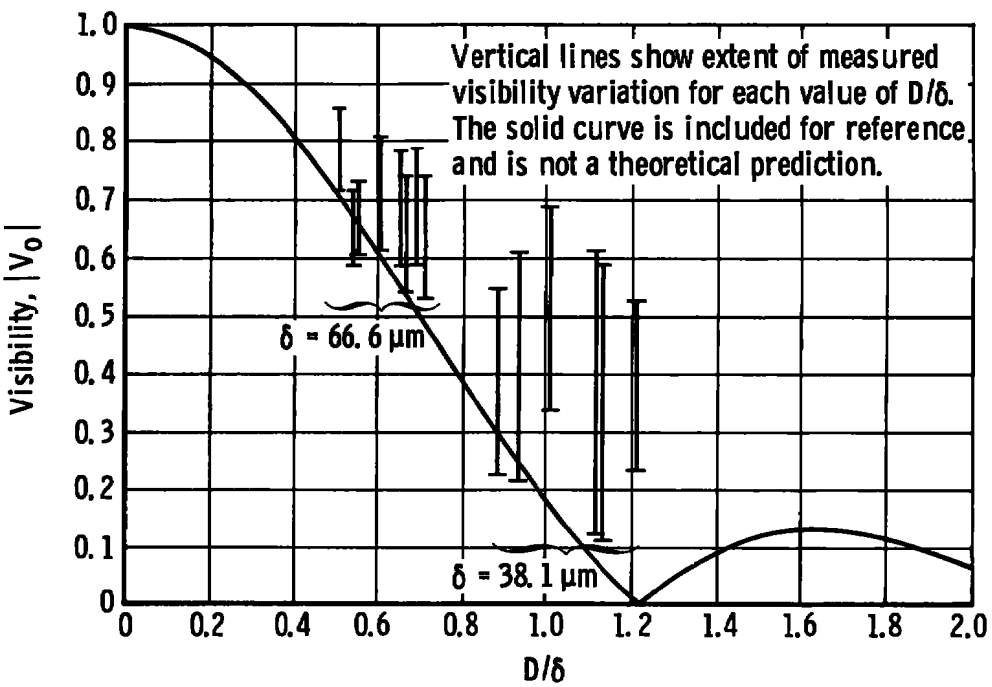

Figure 10. Backscatter data for water drops.

The reason for the wide variation in the backscattered visibilities among particles of the same shape and refractive index and of approximately the same size was not immediately evident. Photodetector shot noise was more noticeable in the back direction than in the forward direction, but the shot noise excursions were of significantly smaller magnitude than the observed visibility variations, and therefore could be eliminated as the cause. It appears that the result of the process of reflection and refraction, which determines the form of the backscattered light in the range of sizes examined, is greatly altered by small changes in the shape or size of the particle. It is probable, for example, that successive water droplets in the stream produced by the droplet generator were

undergoing relatively slow variations in shape and/or size which were too small to be obvious in the microscope or to noticeably affect the forward diffracted light, but which were sufficient to cause the visibilities in the back direction to be widely varied.

It appears that at least for the sizes examined, which were much larger than the wavelength of the illumination, the visibility technique for particle sizing cannot be applied in the case of backscattered light.

3.0 TIME AND FREQUENCY ANALYSIS OF PARTICLE SIZING INTERFEROMETER SIGNALS

3.1 GENERAL

A prerequisite for design of electronics for visibility measurement is time and frequency domain analysis of the scattered light waveform. Time and frequency domain representations of laser velocimeter signals have been discussed (Ref. 11) for scattering particles passing through the center of the probe volume, i.e., through the x-y plane (z = 0) of Fig. 1. The present development will include particles passing anywhere through the probe volume, providing there is no component of velocity in the z direction. Since the electronics includes processing of a signal that is proportional to the waveform visibility, time and frequency analysis of the visibility is included.

3.2 TIME DOMAIN

Equation (9) gives the photodetector output current as a function of the particle's spatial coordinates x, y, and z. To obtain this current as a function of time, it is assumed the particle moves with constant velocity, with x, y, and z coordinates given by

$$x = v_x t$$

$$v = v_y t$$

$$z = z$$

where v_x is the particle's velocity component in the x direction, and v_y is the velocity component in the y direction. Substituting these values into Eq. (9), and introducing a term which allows for fringe movement provided by a Bragg cell, the photodetector current may be written:

$$i_p(t) \sim \exp\left[-\frac{2}{b_o^2}\left(v_x^2 t^2 + v_y^2 t^2 + z^2 a^2/4\right)\right]$$

$$\times \left[\cosh\left[\frac{2}{b_o^2} v_y t z a\right] + V_o \cos(2\pi f_b t + 2\pi v_y t/\delta)\right]$$

which is of the form

$$i_p(t) = Ke^{-cz^2} e^{-at^2} \left[\cosh(bzt) + V_o \cos(2\pi f_s t)\right] \quad (14)$$

where K is a constant of proportionality and where

$$a = 2(v_x^2 + v_y^2)/b_o^2$$

$$b = 2v_y a/b_o^2$$

$$c = a^2/2b_o^2$$

and

$$f_s = f_b + v_y/\delta$$

where f_b is the Bragg cell frequency. The a-c frequency f_s thus is the sum of the Bragg cell frequency f_b and the rate v_y/δ at which the particle would cross stationary fringes. As a numerical example, for v_y = 10 m/s in the direction opposite to fringe movement, δ = 50 μm and f_b = 15 MHz, the a-c frequency f_s generated is 15 MHz + 0.2 MHz = 15.2 MHz. If the particle were moving in the same direction as the fringes, the a-c frequency observed would be 14.8 MHz.

The visibility as a function of time for particles moving parallel to the z = 0 plane is, from Equation (11):

$$V(t) = \frac{V_o}{\cosh(bzt)} \quad (15)$$

Examples of time domain signals are shown in Figs. 2 and 11. The signals shown in Fig. 2 represent photodetector output currents (i.e., plots of Eq. (14) versus time) for particles having different visibilities V_o, all traveling in the y direction, passing through the exact crossover point of the beams (z = 0). The signals shown in Figs. 11a, b, and c represent plots of Eq. (14) versus time for three particles, all having V_o = 0.50, but traveling in the y direction with three different values of z coordinate. In Fig. 11a, the particle passed through the beam crossover point (z = 0); in Fig. 11b, the particle passed somewhat upstream or downstream of the beam crossing point; and in Fig. 11c, the particle passed yet further upstream or downstream from the crossing point. The corresponding visibilities of the waveforms of Figs. 11a, b, and c are shown in Figs. 11d, e, and f, respectively. Except at the crossover point of the beams (z = 0), where the visibility remains constant and equal to V_o, the visibility rises to a maximum value equal to V_o then decreases. The peak visibility V_o is always reached when the particle is in either the z = 0 plane or the y = 0 plane.

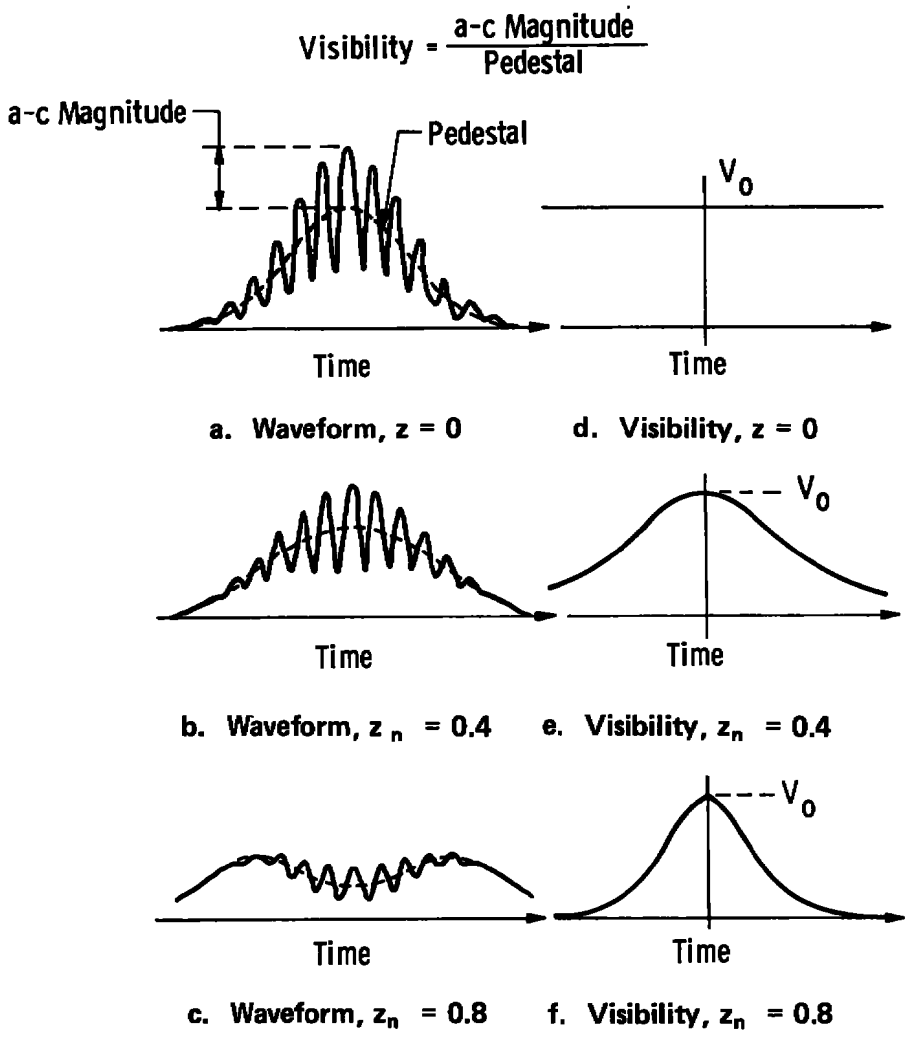

Figure 11. Laser velocimeter waveforms and their corresponding visibilities versus time.

It is useful to define a normalized z coordinate z_n that is equal to unity where the edge of the probe volume intersects the z axis. The intersection of the edge of the probe volume with the z axis is defined (Ref. 12) as the point where the illuminating fringe intensity has decreased to e^{-2} times its value at probe center. This may be shown to occur at $z = 2b_o/a$ for small a. The normalized coordinate z_n is then defined as

$$z_n = (a/2b_o)\, z \tag{16}$$

In terms of z_n, the plots of Fig. 11 are for z_n = 0, 0.4, and 0.8.

3.3 FREQUENCY DOMAIN

The Fourier transform of Eq. (14) gives the frequency spectrum of the photodetector signal. The transform of Eq. (15) gives the visibility spectrum. The pedestal will be considered first, then the a-c term, and finally the visibility. In the time domain the pedestal is, from Eq. (14):

$$i_{ped}(t) = Ke^{-cz^2}e^{-at^2} \cosh(bzt)$$

The Fourier transform may be found with the aid of integral tables (Ref. 13) as

$$I_{ped}(f) = K(\pi/a)^{1/2} \exp\left[-(c - b^2/4a)z^2\right] \exp\left[-\pi^2 f^2/a\right] \cos(\pi bzf/a) \tag{17}$$

This is a frequency dependent Gaussian multiplied by a frequency dependent cosine function. In the z = 0 plane the cosine term is equal to unity, and the spectrum reduces to a pure Gaussian function.

The pedestal bandwidth is theoretically infinite. The bandwidth can be arbitrarily defined, however, using the frequency where the envelope of the spectrum (i.e., the Gaussian factor) has decreased to ten percent of its peak value, and the following can be noted:

1. The pedestal bandwidth is independent of the particle's z coordinate.

2. The pedestal contains frequencies extending to f = 0. This means the pedestal channel in the electronics must be d-c coupled. It is true that a-c coupling through a large capacitor would pass a single pedestal with little noticeable effect. However, removing the d-c component of a periodic waveform causes it to "float down" until there is as much area below the time axis as there is above the time axis, and the effect on a series of random pedestals would be similar.

3. The pedestal bandwith depends on the particle velocity. The bandwidth, designated $f_{10\%}$, may be found from the Gaussian factor in Eq. (17) as

$$\exp\left[-\pi^2 (f_{10\%})^2/a\right] = 0.1$$

$$f_{10\%} = 0.483\,(a)^{1/2}$$

$$= 1.37\, v_p/(2b_o)\ \text{Hz}$$

where $v_p = (v_x^2 + v_y^2)^{1/2}$ is the particle velocity and $2b_o$ is the beam waist diameter.

The a-c component in the time domain is, from Eq. (14):

$$i_{ac}(t) = Ke^{-cz^2} e^{-at^2} V_o \cos(2\pi f_s t) \tag{18}$$

and the Fourier transform is

$$I_{ac}(f) = (KV_o/2)(\pi/a)^{1/2} \exp[-cz^2] \times \left\{\exp[-\pi^2 (f + f_s)^2/a] + \exp[-\pi^2 (f - f_s)^2/a]\right\} \tag{19}$$

This is composed of two Gaussians, one on the positive frequency axis centered at f_s, the other on the negative frequency axis centered at $-f_s$. Except for the translation in frequency and a magnitude factor, each Gaussian is identical to the pedestal spectrum Gaussian. The bandwidth, then, of the a-c component is twice the bandwidth of the pedestal.

The frequency domain representation of the visibility, found by Fourier transforming V(t) given by Equation (15), is

$$V(f) = \frac{V_o \pi}{bz} \frac{1}{\cosh(\pi^2 f/bz)}, \quad |z| > 0 \tag{20}$$

(For z = 0, the visibility is a constant, equal to V_0 and the frequency spectrum is an impulse at f = 0.)

The bandwidth of the visibility signal can be defined in a manner similar to that for the pedestal, i.e., as that frequency where the spectrum has decreased to ten percent of its peak value. The visibility bandwidth $f_{V10\%}$ thus defined is found to be

$$\cosh[\pi^2 (f_{V10\%})/bz] = 10$$

$$f_{V10\%} = 0.303\, bz \text{ Hz} \tag{21}$$

Unlike the pedestal bandwidth, the visibility bandwidth is dependent on the z coordinate. In terms of the normalized coordinate z_n [Eq. 16] the visibility bandwidth may be written:

$$f_{V10\%} = 2.424\, v_y\, z_n/(2b_o) \text{ Hz}$$

Frequency spectra are illustrated in Fig. 12. The positive frequency portion of the pedestal and a-c spectra are shown for two cases: (1) the particle passes through the center of the probe volume (z = 0), and (2) the particle passes at the edge of the probe volume (z_n = 1). Other conditions which were used in making the plots are listed in Fig. 12. It can be seen that electronic filtering can be used to separate the a-c from the

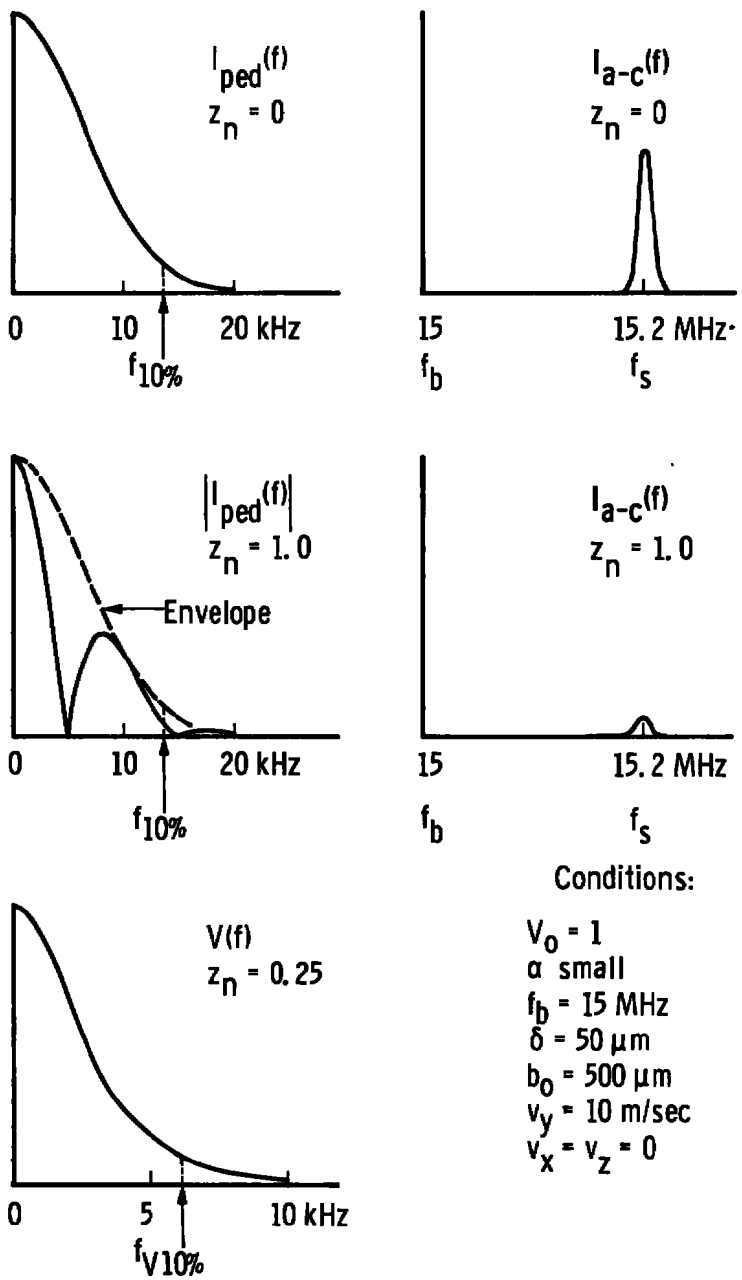

Figure 12. Frequency spectra: pedestal and a-c for z_n = 0, 1.0; visibility for z_n = 0.25.

pedestal provided the a-c frequency f_s is sufficiently large compared to the spectra bandwidths which are in turn proportional to particle velocity.

A plot of the visibility spectrum is also shown for a particle passing with a z coordinate one-fourth of the way from probe center to the edge of the probe volume (z_n = 0.25).

4.0 ELECTRONICS

4.1 GENERAL

The relation of the signal visibility to the size and location of the scattering particle and the collection optics geometry was discussed in Section 2.0. It was noted that if the visibility, given by Eq. (11), is measured when the particle is in either the x-y plane (z = 0) or the x-z plane (y = 0) shown in Fig. 1, then the visibility measured is V_0, a function of the particle size. The subject of this Section is the design of an electronic signal processor to make this measurement.

In a typical laser velocimeter the particles move generally in the y direction (Fig. 1), passing in front of the beam transmitting optics and perpendicular to the fringes. Because of the elongation of the probe volume in the z direction, small particle motion in the z direction can be disregarded. Therefore, the signals and their respective visibilities sketched in Fig. 11 are representative of those to be processed by the electronic circuit under consideration.

Except at the exact crossover point of the beams, where the visibility remains constant and equal to V_0, the signal visibility caused by a passing particle will rise to V_0 and then decrease. For a particle of given size traveling perpendicular to the fringes, this maximum will always be the same, regardless of the point where the particle enters the probe volume, and occurs when the particle crosses the x-z plane at y = 0. This is shown in Figs. 11d, e, and f where the corresponding visibility for each of the signals shown in Figs. 11a, b, and c is plotted.

The manner in which the signal visibility rises to the peak value V_0 to be measured, then falls off, suggests that if an analog electrical signal were generated corresponding to the visibility, then an electronic peak measuring circuit (a "peak detector") could be used to measure the desired peak value.

4.2 VISIBILITY SIGNAL PROCESSOR

Figure 13 contains in block diagram form an electronic circuit which may be used to record the peak visibility. When a particle passes through the fringes, the PM tube signal is amplified and sent simultaneously to a bandpass filter and to a low-pass filter for

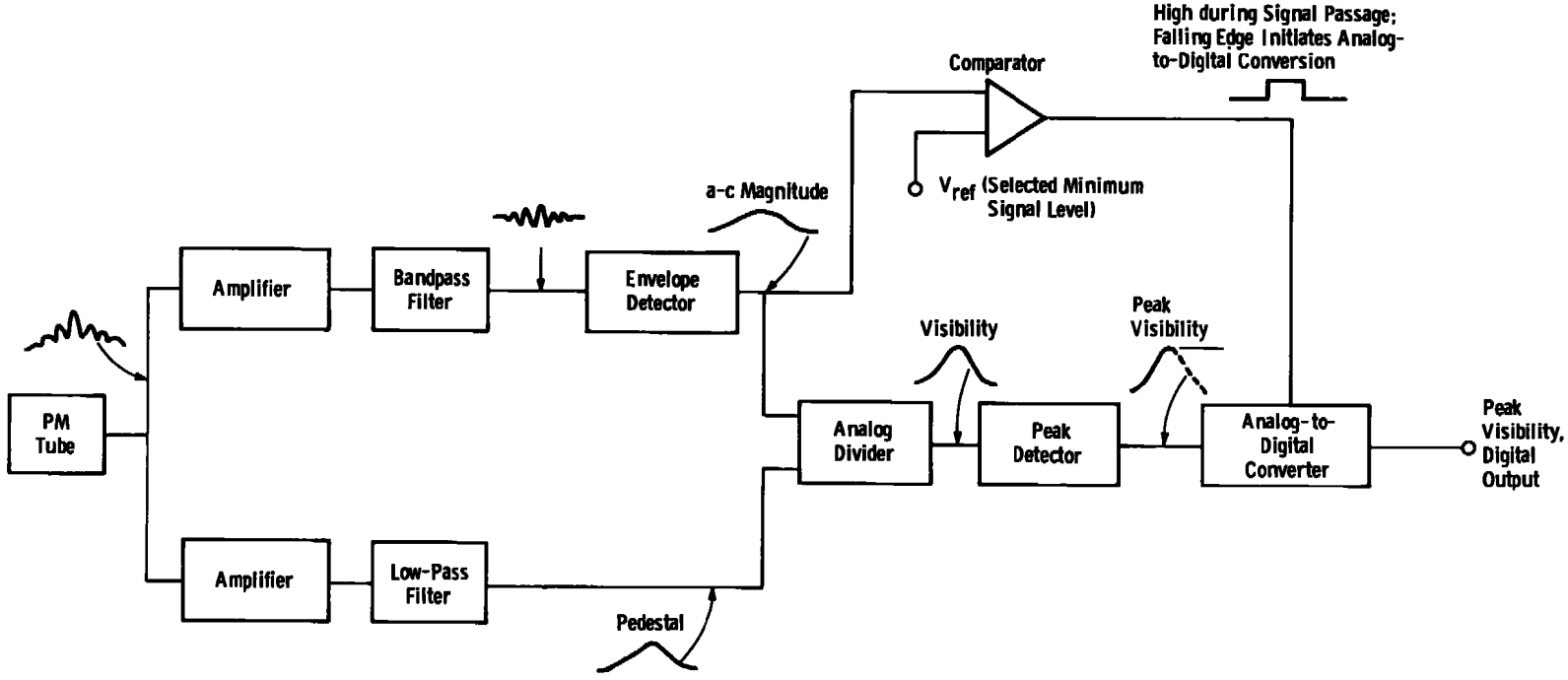

Figure 13. Peak visibility measurement using analog divider, peak detector, and analog-to-digital converter.

separation of the high-frequency a-c component from the low-frequency pedestal. The pedestal signal is fed directly to an analog divider. The a-c component is first envelope-detected to produce a signal proportional to the a-c magnitude then sent to the divider. Care is taken to match time delays through the circuit for the a-c and the pedestal, so that they arrive simultaneously at the divider. The divider's output is a continuous reading of the signal visibility throughout the particle's traversal. The divider is followed by a peak detector to capture the peak value reached. This value is converted to digital form for storage by an analog-to-digital converter until it is ready for output to a data acquisition system.

An electronic processor, based on the block diagram of Fig. 13, was designed and constructed and has been used successfully to measure waveform visibilities in the laboratory. Accuracy of visibility measurement was tested by photographing the processor input waveform from a scattering particle, as it appeared on an oscilloscope screen. The visibility was measured directly from the photograph and then compared with the processor output. It was determined in this manner that the processor accuracy of visibility measurement was within five percent over a visibility range of 0.15 to 1.00.

The circuit of Fig. 13 is limited in its capability to follow fast moving signals by the frequency response of available analog dividers. For a typical optical system, particle velocity must be limited to a few tens of meters per second.

4.3 IMPROVED ELECTRONICS

A proposed alternative circuit for measuring the peak visibility, which is more than an order of magnitude faster and will allow sizing of particles moving at velocities of several hundreds of meters per second, is outlined in Fig. 14 (patent applied for). The circuit can be substituted for the analog divider, peak detector and analog-to-digital converter of Fig. 13, and will read out the visibility V_o in digital form.

The pedestal is followed by a voltage-divider network which divides the full value of the pedestal into a number of equal increments; in the circuit shown, the pedestal is divided into 25 increments. Outputs from the voltage-divider network (passed through high input impedance buffer op-amps) provide voltages that are 0.96 times, 0.92 times, 0.88 times, etc., the full pedestal value. (Only a representative number of the components actually required in the circuit are shown, to simplify the diagram.)

Each such partial pedestal voltage from the divider network goes to one side of a high-speed voltage comparator. The a-c magnitude is fed to the other side of each comparator. As the a-c magnitude rises with respect to the pedestal during signal passage (corresponding to an increasing visibility), it surpasses in sequence each partial pedestal voltage until the peak ratio of the a-c magnitude to pedestal (i.e., the peak visibility) is

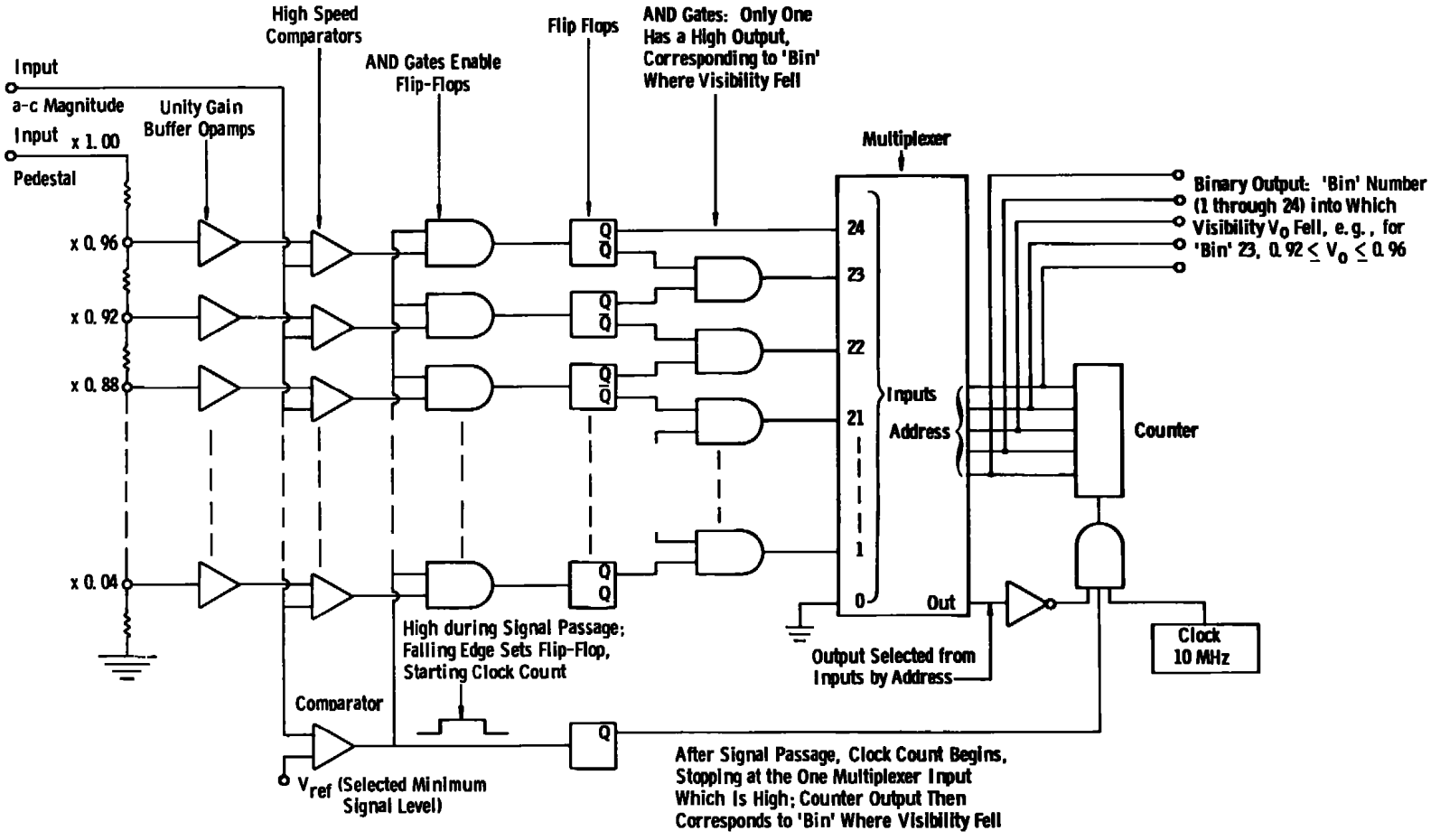

Figure 14. Proposed circuit to replace analog divider, peak detector, and analog-to-digital converter of Fig. 13.

reached. At this point, the output is high for all comparators which are connected to the partial pedestal voltages below that reached by the a-c magnitude. The comparators are followed by AND gates which are wired as shown to pass the comparator outputs only when a selected minimum a-c signal is present, to avoid reading background noise in the absence of a signal.

As a comparator's output goes high it sets the Q output of a corresponding flip-flop, storing that information in digital form. AND gates are connected to the flip-flop complementary outputs as shown so that only the highest set flip- flop's output is passed to the digital multiplexer. Thus only one of the multiplexer's inputs, numbered 1 through 24, is set high, representing a "bin" into which the peak visibility falls. For example, if during signal passage the a-c magnitude rose to 0.89 times the value of the pedestal, then multiplexer input number 22 would be set high, indicating that the visibility fell between 0.88 and 0.92.

After signal passage, the output of a clock is admitted through an AND gate to a counter. The counter binary output addresses the multiplexer, which in turn outputs the multiplexer input addressed. The output is connected back to the clock AND gate through an inverter as shown. The AND gate admits the pulses to the counter only so long as the multiplexer output (and hence the input addressed) is low. Therefore, the count increases until the one input which is high has been addressed. The multiplexer output then goes high, blocking further counting, and the binary address remains at the bin number in which the visibility fell. This bin number is available as a binary output from the processor. A programmed read-only memory (not shown) may be used to convert the bin number to a visibility or size reading.

5.0 CONCLUSIONS

When single, spherical particles of diameter much larger than the wavelength of the illumination pass through the probe volume of a crossed-beam laser velocimeter, the light diffracted in the forward direction may be reliably and accurately used for sizing, provided the collection optics geometry is carefully chosen. The maximum fringe visibility V_o must be measured, which occurs when the particle is in one of the regions of maximum interference between the beams, i.e., in the x-z plane which bisects the laser source beams ($y = 0$), or in the x-y plane where the beams cross ($z = 0$). If all but a negligible portion of the diffracted light is collected and passed to the photodetector, the relationship of the visibility V_o to the ratio D/δ of particle diameter to fringe spacing may be approximated by the closed form curve of Eq. (12). This requires that the light collection aperture be sufficiently large (Fig. 4), and further, that the beam stops be sufficiently small (Fig. 6). The visibility versus D/δ curve predicted by diffraction theory may in any case be determined by numerical evaluation of Eq. (13), where the

integration is carried out over that portion of the collection lens not blocked by beam stops. Care must be taken in the optical system not to further aperture the diffracted light pattern at any point except at the spatial filter formed by the collection aperture and beam stop combination; for example, photomultiplier tubes having a grill in front of the cathode can cause additional, unwanted spatial filtering.

Backscattered light has been found to be unreliable for sizing by this method, at least in respect to the range of particle sizes examined and experimental configuration used.

A forward-scatter optical system and an electronic processor utilizing the circuit outlined in Fig. 14 are presently being built and tested for practical applications at AEDC. The system is designed to study size distribution in the range of 5 to 70 μm.

Further theoretical and experimental studies are required to determine the smallest particle sizes to which the visibility technique of sizing can be applied and to examine the visibility versus size relationship for backscattered light. Although scalar theory does not apply for particle sizes near the illuminating wavelength, analysis based on Mie theory, which includes index of refraction effects and is applicable to spheres in this size range, can be used to examine the problem.

REFERENCES

1. Farmer, W. M. "Measurement of Particle Size, Number Density, and Velocity Using a Laser Interferometer." Applied Optics, Vol. 11, No. 11, November 1972, pp. 2603-2612.

2. Robinson, D. M. and Chu, W. P. "Diffraction Analysis of Doppler Signal Characteristics for a Cross-beam Laser Doppler Velocimeter." Applied Optics, Vol. 14, No. 9, September 1975, pp. 2177-2183.

3. Roberds, D. W. "Electronic Instrumentation for Interferometric Particle Sizing." Ph.D. Dissertation, The University of Tennessee, Knoxville, 1975.

4. Adrian, R. J. and Early, W. L. "Evaluation of LDV Performance Using Mie Scattering Theory." Paper presented at Minnesota Symposium on Laser Anemometry, Bloomington, Minnesota, October 1975.

5. Durst, F. and Eliasson, B. "Properties of Laser Doppler Signals and Their Exploitation for Particle Size Measurements." Paper presented at LDA-Symposium 1975, Copenhagen, Denmark, August 1975.

6. Hong, N. S. and Jones, A. R. "A Light Scattering Technique for Particle Sizing Based on Laser Fringe Anemometry." Journal of Physics D: Applied Physics, Vol. 9, 1976, pp. 1839-1848.

7. Brayton, D. B. "Small Particle Signal Characteristics of a Dual-Scatter Laser Velocimeter." Applied Optics, Vol. 13, No. 10, October 1974, pp. 2346-2351.

8. Born, M. and Wolf, E. Principles of Optics. Pergamon Press Inc., New York, 1965.

9. Goodman, J. W. Introduction to Fourier Optics. McGraw-Hill Book Company, Inc., New York, 1968.

10. Berglund, R. N. and Liu, B. Y. H. "Generation of Monodisperse Aerosol Standards." Environmental Science and Technology, Vol. 7, February 1973, pp. 147-153.

11. Crosswy, F. L. and Hornkohl, J. O. "Signal Conditioning Electronics for a Laser Vector Velocimeter." The Review of Scientific Instruments, Vol. 44, September 1973, pp. 1324-1332.

12. Brayton, D. B. and Goethert, W. H. "A New Dual-Scatter Laser Doppler-Shift Velocity Measuring Technique." ISA Transactions, Vol. 10, No. 1, 1971, pp. 40-50.

13. Gradshtein, I. S. and Ryzhik, I. M. Table of Integrals, Series and Products. Academic Press, New York, 1965.

14. Abramovitz, M. and Stegun, I. A. Handbook of Mathematical Functions. National Bureau of Standards, Washington, D.C., 1964.

APPENDIX A
MATHEMATICAL DERIVATION OF THE SCATTERED LIGHT SIGNAL WAVEFORM

The derivation of Eq. (9) will be outlined using Fraunhofer diffraction theory. The diffraction geometry is shown in Fig. 3. The procedure and assumptions to be used are discussed in Section 2.1. The field diffracted from each source beam is found by integrating the illuminating field of that beam over a circular aperture located in the crossover region of the beams. Babinet's principle is used to show that in the region in the plane of observation which excludes the source illumination, the diffracted intensity distribution calculated will be the same as when the aperture is replaced by an opaque disc. The opaque disc is assumed to satisfactorily approximate a sphere of like diameter.

The fields of the illuminating beams are given by Eqs. (1a) and (1b). The equations may be rewritten in terms of the coordinates x, y, z by using the transformation relations

$$y_1 = y \cos(\alpha/2) - z \sin(\alpha/2)$$

$$y_2 = y \cos(\alpha/2) + z \sin(\alpha/2)$$

$$z_1 = y \sin(\alpha/2) - z \cos(\alpha/2)$$

$$z_2 = -y \sin(\alpha/2) + z \cos(\alpha/2)$$

where α is the beam separation angle.

The illuminating fields become

$$E_1 = A(x, y, z) \exp\left[-i\omega_o t + i(kz + yk\alpha/2)\right] \tag{A-1a}$$

$$E_2 = B(x, y, z) \exp\left[-i\omega_o t + i(kz - yk\alpha/2)\right] \tag{A-1b}$$

where

$$A(x, y, z) = E_o \exp\left[-(x^2 + y^2 - yz\alpha + z^2\alpha^2/4)/b_o^2\right]$$

$$B(x, y, z) = E_o \exp\left[-(x^2 + y^2 + yz\alpha + z^2\alpha^2/4)b_o^2\right]$$

In these equations, sin α has been approximated by α and cos α by unity.

In accordance with assumption 2 in Section 2.1, in the integration of the fields over the aperture representing the particle, the amplitude terms A(x,y,z) and B(x,y,z) of these equations will be considered constants, equal to their values at (x_c,y_c,z_c), the coordinates

of the particle center. In the phase terms of these equations, the coordinate y will be replaced by $(y_c + y')$, where integration will be with respect to x' and y', rectangular coordinates with origin at the aperture center. Further, using Eq. (2) to let $ka = 2\pi/\delta$, the fields to be integrated finally become

$$E_1 = A(x_c, y_c, z_c) \exp\left\{-i\omega_o t + i\left[kz - \pi(y_c + y')/\delta\right]\right\} \quad \text{(A-2a)}$$

$$E_2 = B(x_c, y_c, z_c) \exp\left\{-i\omega_o t + i\left[kz - \pi(y_c + y')/\delta\right]\right\} \quad \text{(A-2b)}$$

The diffracted field due to each of these illuminating fields is found by an integration over the aperture which is equivalent to finding the two-dimensional Fourier transform (Ref. 9) of the illuminating field, evaluated at frequencies $f_x = x_o/\lambda_o R$ and $f_y = y_o/\lambda_o R$, where R is the distance from the aperture to the plane of the collection lens and x_o, y_o are coordinates centered on the collection lens.

Examination of Eqs. (A-2a) and (A-2b) shows that each contains components that will be constant in the integration. The first equation has the phase factor $\exp(i\pi y'/\delta)$ and the second has the phase factor $\exp(-i\pi y'/\delta)$. The shift theorem of Fourier transform theory states that the transform of a function which is multiplied by a phase term in the object plane is simply spatially shifted in the observation plane.

The problem for each beam reduces to finding the Fourier transform of a uniform field illuminating a circular aperture and then shifting the diffracted field in the observation plane. The desired diffracted fields are well known in this case (Ref. 9); they are simply Airy patterns which are spatially shifted in the observation plane and are written as follows:

$$E_{s1} = -i\, A(x, y, z)\ (kD^2/8R) \exp\left[ikR + ikr_o^2/2R\right]$$

$$\times \exp\left[-i\omega_o t + i(kz + \pi y/\delta)\right] \left[\frac{2J_1(\beta r_1)}{\beta r_1}\right] \quad \text{(A-3a)}$$

$$E_{s2} = -i\, B(x, y, z)\ (kD^2/8R) \exp\left[ikR + ikr_o^2/2R\right]$$

$$\times \exp\left[-i\omega_o t + i(kz - \pi y/\delta)\right] \left[\frac{2J_1(\beta r_2)}{\beta r_2}\right] \quad \text{(A-3b)}$$

For simplicity of notation, the coordinates of the particle's location x_c, y_c, z_c have been replaced by x, y, z. The functions A(x,y,z) and B(x,y,z) are those previously defined, and

$$r_o^2 = x_o^2 + y_o^2$$

$$r_1^2 = x_o^2 + (y_o - s/2)^2$$

$$r_2^2 = x_o^2 + (y_o + s/2)^2$$

$$s = \lambda R/\delta$$

$$\beta = kD/2R = \pi(D/\delta)/s$$

The fields E_{s1} and E_{s2} may now be substituted into Eq. (5), giving

$$i_p \sim \exp\left[-\frac{2}{b_o^2}(x^2 - y^2 + z^2\alpha^2/4)\right] \times \left\{\exp(2yz\alpha/b_o^2)\int_o^{2\pi}\int_o^{L/2}\left[\frac{J_1^2(\beta r_1)}{(\beta r_1)^2}\right] r_o\, dr_o\, d\psi + \exp(-2yz\alpha/b_o^2)\int_o^{2\pi}\int_o^{L/2}\left[\frac{J_1^2(\beta r_2)}{(\beta r_2)^2}\right] r_o\, dr_o\, d\psi + 2\cos(2\pi y/\delta)\int_o^{2\pi}\int_o^{L/2}\left[\frac{J_1(\beta r_1)}{(\beta r_1)}\,\frac{J_1(\beta r_2)}{(\beta r_2)}\right] r_o\, dr_o\, d\psi\right\} \quad \text{(A-4)}$$

The limits of integration shown are for a circular lens centered on the optical axis and neglect beam stops.

A simplification of this result is obtained if it is noticed that because of the symmetry involved,

$$\int_o^{2\pi}\int_o^{L/2}\frac{J_1^2(\beta r_1)}{(\beta r_1)^2} r_o\, dr_o\, d\psi = \int_o^{2\pi}\int_o^{L/2}\frac{J_1^2(\beta r_2)}{(\beta r_2)^2} r_o\, dr_o\, d\psi \quad \text{(A-5)}$$

This permits rewriting Eq. (A-4) as

$$i_p \sim \exp\left[-\frac{2}{b_o^2}(x^2 + y^2 + z^2\alpha^2/4)\right] \times \left\{\cosh(2yz\alpha/b_o^2)\int_o^{2\pi}\int_o^{L/2}\left[\frac{J_1^2(\beta r_1)}{(\beta r_1)^2} + \frac{J_1^2(\beta r_2)}{(\beta r_2)^2}\right] r_o\, dr_o\, d\psi + 2\cos(2\pi y/\delta)\int_o^{2\pi}\int_o^{L/2}\left[\frac{J_1(\beta r_1)}{\beta r_1}\,\frac{J_1(\beta r_2)}{\beta r_2}\right] r_o\, dr_o\, d\psi\right\} \quad \text{(A-6)}$$

Dividing through the right side of this proportionality by

$$\int_0^{2\pi} \int_0^{L/2} \left[\frac{J_1^2(\beta r_1)}{(\beta r_1)^2} + \frac{J_1^2(\beta r_2)}{(\beta r_2)^2} \right] r_o \, dr_o \, d\psi$$

provides a convenient normalization, thus allowing the expression for i_p to be written as Eq. (9).

APPENDIX B
NUMERICAL EVALUATION OF THE VISIBILITY

Numerical evaluation of Eq. (13) for the visibility V_o is straightforward, using well-known programming techniques for evaluating double integrals. Some helpful things to consider when writing the program are discussed here.

It should be noted first that because of the symmetry involved, the integration need be performed over one quadrant only. i.e., the angular limits of integration may be from 0 to $\pi/2$ rather than from 0 to 2π.

A second consideration is efficient evaluation of the first order Bessel function, $J_1(x)$. This function may be written as a polynomial approximation, for example as in Ref. 14, page 370, Expression 9.4.4. which is of the form

$$J_1(x) = C_o x + C_1 x^3 + C_2 x^5 + \ldots + C_6 x^{13}$$

Such an expression should be programmed as

$$J_1(x) = ((((((C_6 x^2 + C_5)\, x^2 - C_4)\, x^2 - C_3)\, x^2 + C_2)\, x^2 + C_1)\, x^2 + C_o)\, x$$

for greater speed and to minimize round-off error. This expression is good for values of the argument $0 \leqslant x \leqslant 3$. For values of the argument $x > 3$, the polynomial approximation of Expression 9.4.6, page 370 of Ref. 14 was used.

A final note here is the radial limits of integration in Eq. (13) with beam stops. For a single, central beam stop the lower radial limit is simply changed from zero to the dimensionless beam stop radius (p/2)/s:

$$\int_o^{\pi/2} \int_{(p/2)/s}^{(L/2)/s} du\, d\psi$$

The geometry for the twin beam stop case is shown in Fig. B-1. The integration is performed as:

$$\int_o^{\psi_1} \left\{ \int_o^{R_1/s} du + \int_{R_2/s}^{(L/2)/s} du \right\} d\psi + \int_{\psi_1}^{\pi/2} \int_o^{(L/2)/s} du\, d\psi$$

where

$$u = r_o/s$$

$$\psi_1 = \arctan \frac{(p/2)}{\left[(s/2)^2 - (p/2)^2\right]^{1/2}}$$

$$R_1 = (s/2) \cos \psi - \left[(p/2)^2 - (s/2)^2 \sin^2 \psi\right]^{1/2}$$

$$R_2 = (s/2) \cos \psi + \left[(p/2)^2 - (s/2)^2 \sin^2 \psi\right]^{1/2}$$

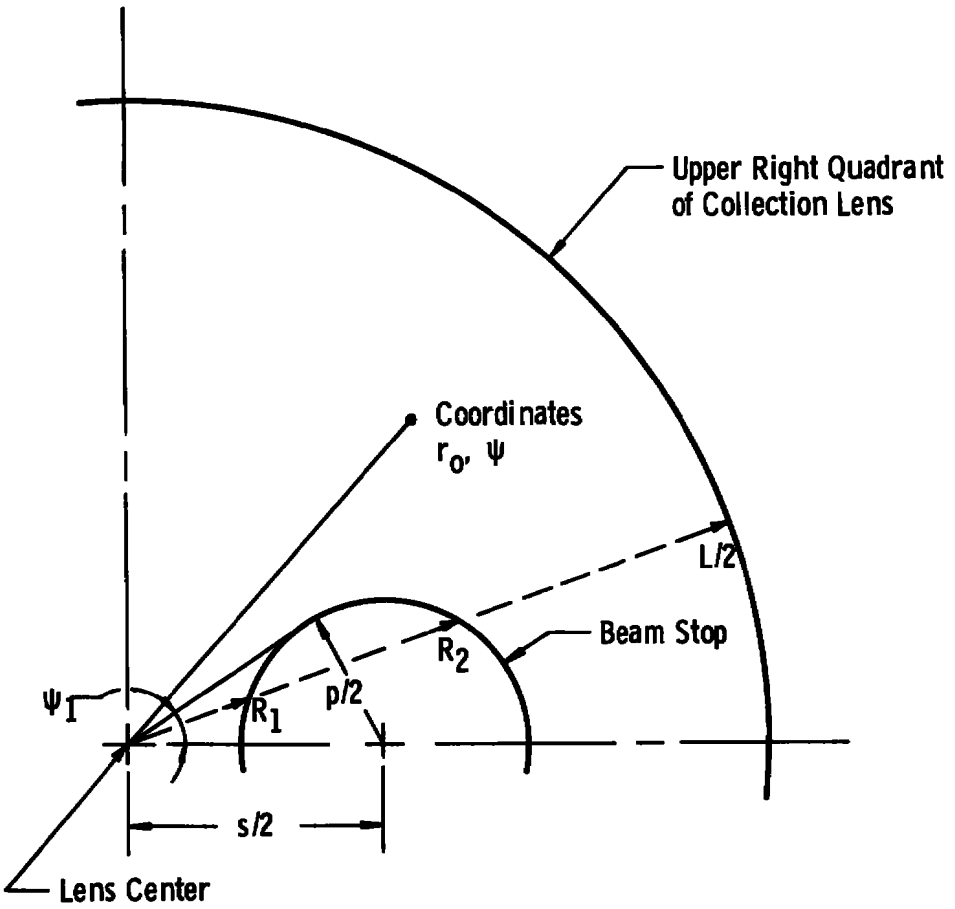

Figure B-1. Twin beam stop geometry for numerical evaluation of visibility.